J. Phys. C: Solid State Phys., **14** (1981) 665–683. Printed in Great Britain

Numerical investigation of the $(s + p) \otimes T_{1u}$ system: I. Vibronic eigenstates and absorption spectra

Ulrich Grevsmühl†
Department of Theoretical Physics, 1 Keble Road, Oxford, UK

Received 9 September 1980

Abstract. The eigenvalue problem of the ideal $(s + p) \otimes T_{1u}$ pseudo-Jahn–Teller system is solved by numerical diagonalisation of the energy matrix. Low- and high-energy vibronic eigenstates, absorption lines and spectra at zero temperature are computed for representative values of the electronic 2s–2p spacing in all coupling regimes. In addition the semiclassical absorption lineshape function is calculated: best agreement with the absorption spectra is found for strong coupling. The computational results suggest especially for high energies a factorisation of the vibronic eigenstates for all coupling strengths. A reclassification of the vibronic states is then useful, which provides a link with the adiabatic energy surfaces, enabling a unified description of the absorption spectra. The system exhibits an optical resonance effect, and the calculations show under what conditions this effect can be neglected.

1. Introduction

Molecules and crystalline defects having a symmetrical configuration of nuclei and involving nearly degenerate electronic states which are coupled by vibrational modes are often referred to as pseudo-Jahn–Teller (abbreviated as pJT) systems. In particular, in cubic symmetry electronic 2s (A_{1g}) and 2p (T_{1u}) states can interact via a triply degenerate odd-parity T_{1u} vibrational mode. A general solution to this problem has been given by Ham (1973) and the low-energy eigenstates have been investigated extensively in both the weak and strong coupling regions (Ham and Grevsmühl 1973). Furthermore, O'Brien (1976) developed a method based on the WKB approximation to give the wavefunctions and energy levels of the high-energy eigenstates. A numerical calculation is therefore desirable to verify the predicted results and to link up the various parts of the theory. This has partially been done by Kayanuma and Toyozawa (1976) for the low-lying energy levels and by Kayanuma and Kojima (1980) for some of the optical absorption spectra.

The purpose of the present and following paper is to close the still existing gap and to investigate the $(s + p) \otimes T_{1u}$ system along similar lines to those used for the ideal Jahn–Teller systems. The vibronic eigenstates can be separated into two non-mixing sets, one of which is independent of the coupling strength. The eigenvalue problem of the other set is solved by numerical diagonalisation of the energy matrix in all coupling regimes up to the highest energies. Under certain conditions it is useful to classify this second set of vibronic states in three further sets, type *A*, *B*, and *C* states, which can be

† Present address: Pädagogische Hochschule Freiburg, Kunzenweg 21, 7800 Freiburg/Br., West Germany.

0022-3719/81/050665 + 19 $01.50

associated with the adiabatic energy surfaces of the static problem. The strengths of the absorption lines as functions of coupling strength and the absorption spectra at zero temperature are calculated and described by means of the type A, B and C states. In addition the absorption lineshape function is calculated in the semiclassical approximation.

2. Ideal $(s + p) \otimes T_{1u}$ pseudo-Jahn–Teller system

2.1. Model Hamiltonian

Our model Hamiltonian consists of the vibrational part H_L, the electronic part H_e and the vibronic interaction term H_{pJT} and can be expressed as

$$H = H_L + H_e + H_{pJT}$$

where

$$H_L = \tfrac{1}{2}(p^2 + q^2), \qquad H_e = \delta\rho_0, \qquad H_{pJT} = (2)^{1/2}\kappa \sum_{i=x,y,z} q_i\rho_i. \tag{1}$$

q_j and $p_j = -\mathrm{i}\mathrm{d}/\mathrm{d}q_j$ $(j = x, y, z)$ are the dimensionless coordinates and momentum conjugates which satisfy the commutation rule $[p_j, q_k] = \mathrm{i}\delta_{jk}$. Furthermore

$$p^2 = \sum_{i=x,y,z} p_i^2 \qquad \text{and} \qquad q^2 = \sum_{i=x,y,z} q_i^2.$$

In the configuration of cubic symmetry $(q_x = q_y = q_z = 0)$ the excited electronic singlet state $|2s\rangle$ is taken to have an energy 2δ relative to the excited triplet state $|x\rangle$, $|y\rangle$, $|z\rangle$. The Hermitian electronic operators are given by

$$\rho_0 = |2s\rangle\langle 2s| - \sum_{i=x,y,z} |i\rangle\langle i|$$

$$\rho_i = |i\rangle\langle 2s| + |2s\rangle\langle i| \qquad (i = x, y, z). \tag{2}$$

Both the parameter δ of the electronic 2s–2p separation and the coupling coefficient κ are dimensionless quantities. δ is related to the actual energy difference E_{sp} of the two excited states by $\delta = E_{sp}/2\hbar\omega$, where $\hbar\omega$ is the energy quantum of the vibrational T_{1u} mode.

2.2. Static problem

The eigenvalue problem for our model Hamiltonian H can easily be solved when we omit the ionic kinetic energy $(p^2 = 0)$. This corresponds to a completely static treatment of the lattice where the dependence of the various lattice coordinates is taken only parametrically. The linear combinations of the electronic states that diagonalise H for any choice of q_x, q_y, q_z are found by solving the secular equation (Ham 1973).

Two of the states are linear combinations of 2s and 2p and have the energies

$$\varepsilon_{1,2} = \tfrac{1}{2}q^2 \pm (\delta^2 + 2\kappa^2 q^2)^{1/2}. \tag{3}$$

The two other states which correspond to the double root of the secular equation involve the 2p states alone

$$\varepsilon_{3,4} = \tfrac{1}{2}q^2 - \delta. \tag{4}$$

The adiabatic energy surfaces (3) and (4) have spherical symmetry in q-space and are depicted for representative cases in figure 1. Note that $\varepsilon_{1,2}$ and $\varepsilon_{3,4}$ do not depend on the sign of δ and κ, respectively.

It is convenient to introduce the stabilisation energy

$$\varepsilon_G = \kappa^2 \tag{5}$$

Provided the coupling is sufficiently strong, so that $2\varepsilon_G > |\delta|$, a well develops with the minimum at $q = q_0 > 0$ and the energy $\varepsilon_{min}(q = q_0) = -\varepsilon_G[1 + (\delta/2\varepsilon_G)^2]$.

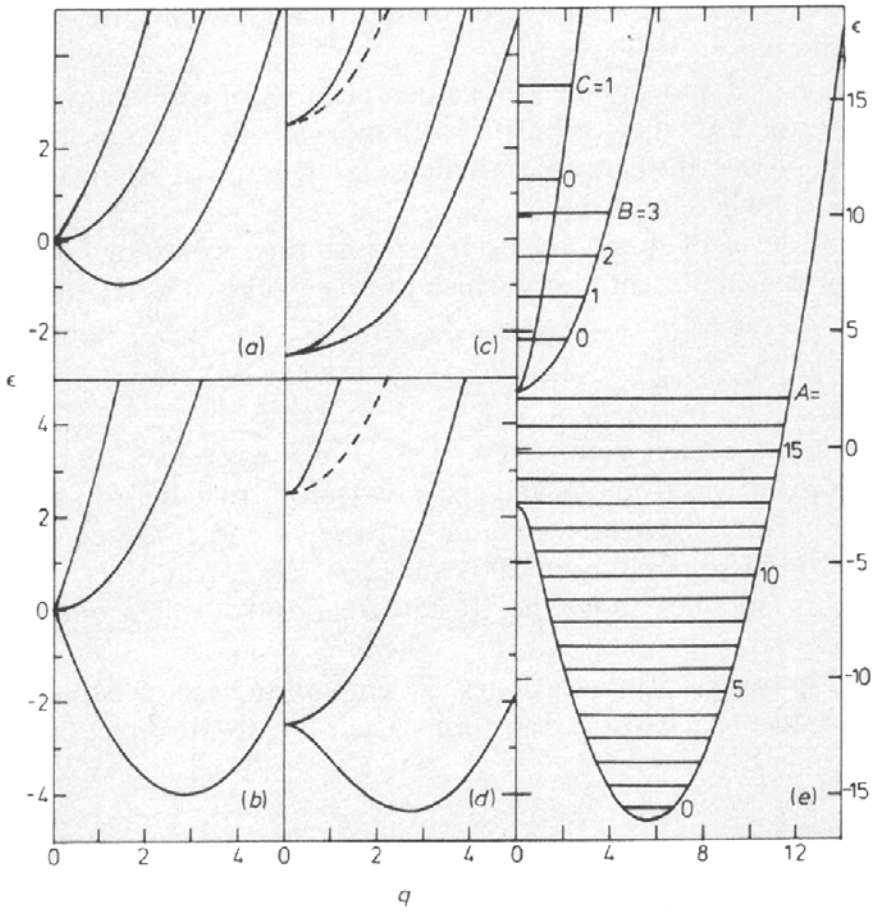

Figure 1. Adiabatic energy surfaces: (*a*) $\delta = 0$, $\varepsilon_G = 1$, (*b*) $\delta = 0$, $\varepsilon_G = 4$, (*c*) $\delta = \pm\frac{5}{2}$, $\varepsilon_G = 1$, (*d*) $\delta = \pm\frac{5}{2}$, $\varepsilon_G = 4$, (*e*) $\delta = -\frac{5}{2}$, $\varepsilon_G = 16$. The energy surfaces have spherical symmetry in q-space. The doubly degenerate middle energy surfaces depend on the sign of δ: broken lines in (*c*) and (*d*) indicate these energies for $\delta = -\frac{5}{2}$. In (*e*) the lowest-lying type A, B and C energy levels for $J = 1$ (see §3.2) have been drawn.

For weaker coupling ($2\varepsilon_G \leqslant |\delta|$) the minimum occurs at $q = 0$ and is given by $\varepsilon_{min}(q = 0) = -|\delta|$. In this case no well develops.

When the electronic states are accidentally degenerate ($\delta = 0$), the resulting instability involves a linear splitting of the electronic degeneracy exactly as in the Jahn–Teller effect, and a well of depth $(-\varepsilon_G)$ develops even for weak coupling.

2.3. Vibronic eigenstates

The spherical symmetry of the static problem is a result of the model Hamiltonian H being invariant under a continuous group of simultaneous rotations of the electronic

and vibrational coordinates. The total angular momentum operator $\boldsymbol{J} = \boldsymbol{L} + \boldsymbol{l}$ therefore commutes with the vibronic interaction term and thus with the model Hamiltonian H but neither the vibrational angular momentum operator $\boldsymbol{L}$ nor the electronic orbital angular momentum operator $\boldsymbol{l}$ do. Furthermore, the total inversion operator $\Lambda = I\rho_0$ also commutes with H and $\boldsymbol{J}$, where I is the inversion operator in q-space and the electronic inversion operator ρ_0 is given by equation (2). Ham (1973) has used these symmetry properties to give a general solution for the dynamic problem by classifying the states by the quantum numbers J, $J_z = M$ and the parity Λ' and separating them into two non-mixing sets. For a numerical investigation of this system, his approach is not convenient, however, as it leads to a set of coupled differential equations which are difficult to solve.

Instead, as H_L, $\boldsymbol{L}^2$ and L_z constitute a complete set of commuting observables, it is of advantage to use the complete orthonormal set of eigenvectors $|nLm\rangle \equiv |(2N + L)Lm\rangle$ of the 3D isotropic oscillator as vibrational states with the energies $\varepsilon_L = 2N + L + \frac{3}{2}$ where $N, L = 0, 1, 2, \ldots$.

A complete level of degenerate states transforms according to the symmetrical product $[n]$ of their representations, which can be expressed as (Heine 1964, p 258)

$$[n] = \sum_{L = 0, 2 \text{ or } 1, 3}^{n} D_L \tag{6}$$

where $L = 0, 2, \ldots, n$ if n is even, or $L = 1, 3, \ldots, n$ if n is odd.

Furthermore, the electronic 2s and 2p states transform under rotation as $\mathrm{D}_l (l = 0, 1)$ and the orthonormal eigenvectors common to H_e, $\boldsymbol{l}$ and l_z are given by $|n_e lm\rangle$. The eigenvalues of H_e corresponding to $|200\rangle$ and $|21m\rangle$ are $+\delta$ and $-\delta$, respectively. Thus, the electronic 2s state lies above the 2p state for positive values of δ and below it for negative values of δ.

Taking these two sets of basis states, we employ the vector coupling theorem and construct a product space which transforms according to the direct product

$$[n] \times \mathrm{D}_l = \sum_L (\mathrm{D}_{L+l} + \mathrm{D}_{L+l-1} + \ldots + \mathrm{D}_{|L-l|}).$$

From the range of L values given by a certain vibrational quantum number n according to (6), we can pick out those values of L the direct product of which with l leads to a reduction containing D_J. With the vector coupling theorem we find that L can take only the values $L = J + 1, J, J - 1$ for $l = 1$ (and $J \geqslant 1$; $L = 1$ for $J = 0$) and $L = J$ for $l = 0$.

The orthonormalised vibronic functions belonging to the component M of the D_J representation can now be formed with the help of the vector addition coefficients (Messiah 1969, p 1054)

$$\begin{aligned} |JM, (J + 2N)J, 2\mathrm{s}\rangle &= |(J + 2N)JM\rangle\,|200\rangle \\ |JM, (L + 2N)L, 2\mathrm{p}\rangle &= \sum_{m = -1, 0, 1} \langle L1(M - m)m|JM\rangle\,|(L + 2N)L(M - m)\rangle\,|21m\rangle \end{aligned} \tag{7}$$

with the energies $\varepsilon(\mathrm{s}) = J + 2N + \frac{3}{2} + \delta$ and $\varepsilon(\mathrm{p}, L) = L + 2N + \frac{3}{2} - \delta$ where $L = J + 1, J, J - 1$ for $J \geqslant 1$ and $L = 1$ for $J = 0$. Note that the 2p states corresponding to $L = J$ and $L = J - 1$ are defined only for $J \geqslant 1$.

Furthermore, as the pseudo-Jahn–Teller term H_{pJT} has *even* parity in the combined electronic and vibrational space, it can mix only those states of (7) to form vibronic

eigenstates transforming as D_J which have the *same* parity. This then leads us to distinguish between two types of eigenfunctions.

Type-I vibronic eigenfunctions of H which belong to J, M and have parity $\Lambda' = (-1)^J$ can now be expressed as

$$\begin{aligned}\Psi^{JM}_{\mathrm{I},j} = \sum_{N=0}^{\infty} [&a(J,j,J+2N)\,|JM,(J+2N)J,2\mathrm{s}\rangle \\ &+ b(J,j,J+2N+1)\,|JM,(J+2N+1)(J+1),2\mathrm{p}\rangle \\ &+ c(J,j,J+2N-1)\,|JM,(J+2N-1)(J-1),2\mathrm{p}\rangle] \end{aligned} \tag{8}$$

where the principal quantum number $j = 0, 1, 2, \ldots$ classifies states with the same J, M. For $J = 0$ the last term is absent: $c(0, j, 2N - 1) \equiv 0$. The $(2J + 1)$-fold degenerate energy eigenvalues of H which correspond to (8) are denoted by $\varepsilon_\delta(\mathrm{I}, jJ)$.

The normalisation of (8) reads

$$\sum_{N=0}^{\infty} [|a(J,j,J+2N)|^2 + |b(J,j,J+2N+1)|^2 + |c(J,j,J+2N-1)|^2] = 1.$$

The summation over the first term represents the total admixture of the s–J states of (7). Similarly, the total admixtures of the p–$(J + 1)$ and p–$(J - 1)$ states of (7) are given by the summations over the second and third terms respectively.

On the other hand we find that the vibronic eigenstates with parity $\Lambda' = (-1)^{J+1}$ consist purely of the p–J states of (7) and are therefore completely independent of H_{pJT}. Type-II vibronic eigenfunctions of H belonging to J, M and $\Lambda' = (-1)^{J+1}$ can thus simply be expressed as

$$\Psi^{JM}_{\mathrm{II},N} = |JM,(J+2N)J,2\mathrm{p}\rangle \tag{9}$$

with the energies $\varepsilon_\delta(\mathrm{II}, NJ) = J + 2N + \frac{3}{2} - \delta$. There are no type-II states for $J = 0$.

The matrix elements of the vibronic interaction term within the space of the vibronic basis states (7) can now be calculated by applying the irreducible tensor method and the Wigner–Eckart theorem to the rotation group in three dimensions. For this purpose it is convenient to express the vibrational and electronic parts of H_{pJT} in terms of irreducible tensor operators and to calculate their reduced matrix elements. We shall not give details of this calculation as it has already been reported elsewhere (Wybourne 1974, §20.6, Kayanuma and Toyozawa 1976, Grevsmühl 1976) but shall merely give the general form of the matrix elements

$$\begin{aligned}&\langle JM,(J+2N-1)(J-1),2\mathrm{p}|H_{\mathrm{pJT}}|JM,(J+2N)J,2\mathrm{s}\rangle \\ &\qquad = \kappa[J(2J+1+2N)/(2J+1)]^{1/2} \\ &\langle JM,(J+2N+1)(J+1),2\mathrm{p}|H_{\mathrm{pJT}}|JM,(J+2N)J,2\mathrm{s}\rangle \\ &\qquad = -\kappa[(J+1)(2J+3+2N)/(2J+1)]^{1/2} \\ &\langle JM,(J+2N-1)(J+1),2\mathrm{p}|H_{\mathrm{pJT}}|JM,(J+2N)J,2\mathrm{s}\rangle \\ &\qquad = \kappa[(J+1)2N/(2J+1)]^{1/2} \\ &\langle JM,(J+2N+1)(J-1),2\mathrm{p}|H_{\mathrm{pJT}}|JM,(J+2N)J,2\mathrm{s}\rangle \\ &\qquad = -\kappa[2J(N+1)/(2J+1)]^{1/2}. \end{aligned} \tag{10}$$

The eigenvalue equation for the type-I states can now be set up. Multiplication from the left with the bra states of (7) yields an infinite set of equations which are coupled

by the coefficients a, b, and c of the eigenvector. Expressing these equations in matrix form, we find a symmetrical band matrix with in general two off-diagonal elements on either side. The eigenvalue problem is solved by numerical diagonalisation of the energy matrix. The computations were carried out on the Oxford ICL 1906A computer by making use of the relevant subroutines of the Nottingham Alogorithms Group.

3. Vibronic eigenstates

3.1. Low-energy eigenstates

Figures 2 show the lowest vibronic energy levels as a function of the coupling strength $(\varepsilon_G)^{1/2}$ for representative values of the parameter δ. Note that type-II energy levels are independent of ε_G.

In the strong-coupling region a strict ordering of the type-I energy levels belonging to the same principle quantum number j according to their J-values is found, as has been predicted by Ham (1973) and also found by Kayanuma and Toyozawa (1976). Consequently, a crossing of the levels may take place at weak or intermediate coupling. In particular, a crossing of the two lowest states with $j = 0$, $J = 0$ and $J = 1$ can occur only for $\delta > 0$, i.e. when the $J = 1$ state is below the $J = 0$ state at zero coupling strength.

An expression for the energies of the lowest type-I states in the strong-coupling region is found by an evaluation of the numerical data

$$\varepsilon_\delta(I, jJ) = j + \tfrac{1}{2} - \varepsilon_G + (J^2 + J + 1 - \delta^2)/4\varepsilon_G \tag{11}$$

which holds well for $\varepsilon_G \gtrsim 4$ and $|\delta| \lesssim 5$, where $j, J = 0, 1, 2, \ldots$, but not too large. It is interesting to note that for $\delta = -1, j = J = 0$ equation (11) is the *exact* expression for all coupling strengths. Equation (11) is in agreement with an expression for the relative energies of the low-energy states in the strong-coupling limit ($2\varepsilon_G \gg |\delta|, \varepsilon_G \gg 1$) predicted by Ham (1973) (see also equation (15) of Grevsmühl (1981)) and is also consistent with an analytical formula recently obtained by Pooler (1980).

Our computational data also confirm Ham's strong-coupling formulae for the total admixtures of the s–J, p–$(J + 1)$, and p–$(J - 1)$ states (7) in the type-I states (8). As expected, best agreement is found for $\varepsilon_G \gtrsim 4$, small $|\delta|$ and j, J not too large.

3.2. High-energy states—Type A, B, C states

A further classification of the type-I states proves particularly useful for large values of $|\delta|$ and provides a link with the adiabatic energy surfaces. Figures 3 show the vibronic energy levels for $J = 1$ as a function of the coupling strength for $\delta = \pm\frac{5}{2}$, which are crucial for the interpretation of the absorption spectra in §4. From these graphs and others for different J and δ we draw the following conclusions.

3.2.1. Type-I energy levels with given J exhibit a *tendency to cross* which appears to be strongest at high energies and for large $|\delta|$. More specific, in the case of $\delta \ll -\frac{1}{2}$ a strong tendency to cross is found for all energy levels involved and in the case of $\delta \gg \frac{1}{2}$ for the high-energy states. Although the levels with the same J actually never cross, as the wavefunctions do not factorise, it is reasonable to regard them as crossed when the tendency is strong and to investigate the behaviour and properties of these new states. For general δ and J, type-I states may then be divided into the three groups A, B, and C, each of which carries its own set of principal quantum number in place of j.

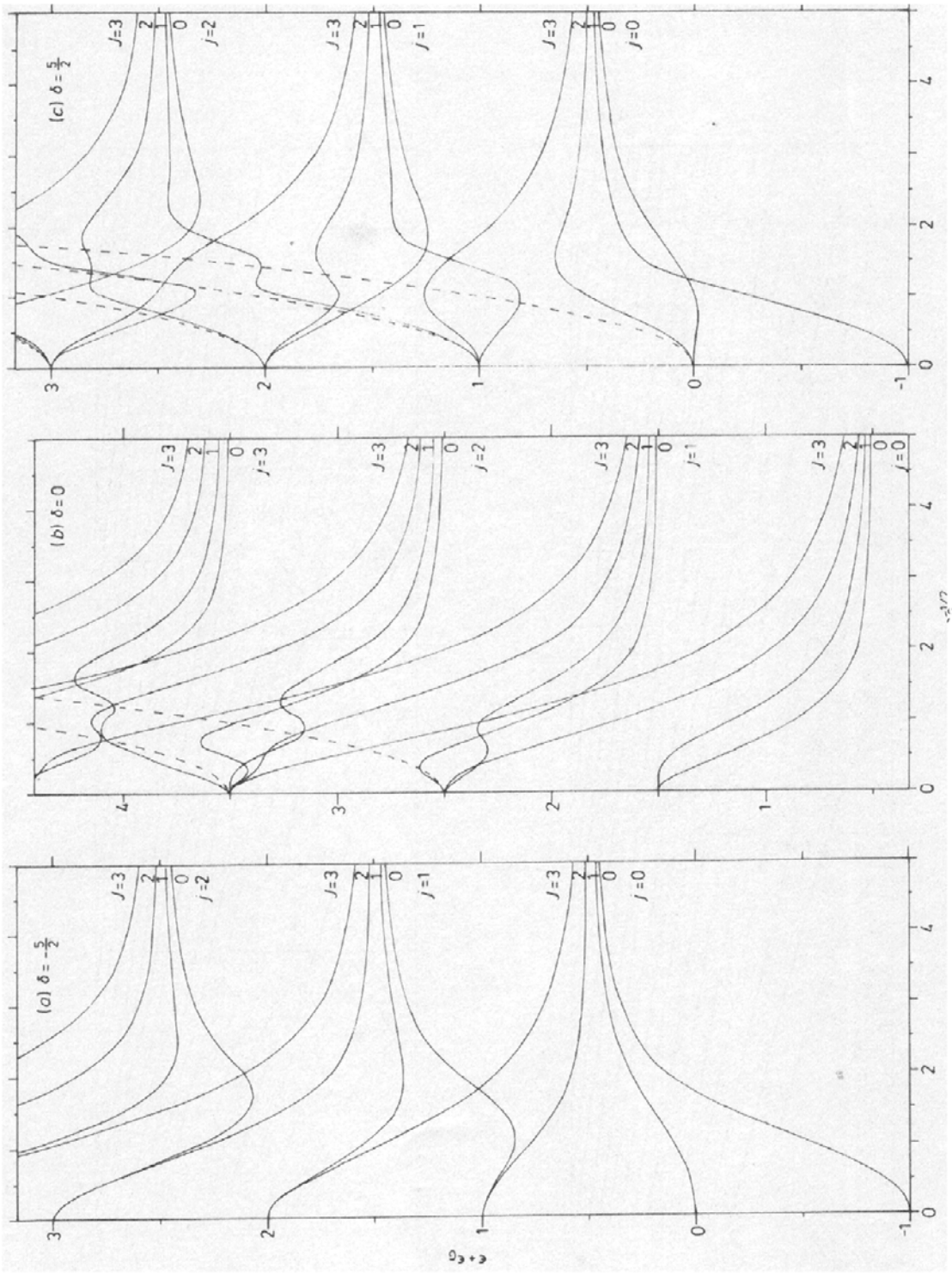

Figure 2. Lowest vibronic energy levels with $J \leqslant 3$, $j \leqslant 2$ or 3 versus coupling strength $\varepsilon_G^{1/2}$ for $\delta = -\frac{5}{2}$ (*a*), $\delta = 0$ (*b*), $\delta = \frac{5}{2}$ (*c*). The parameter δ of the electronic 2s–2p spacing is defined in §2.1. The stabilisation energy $\varepsilon_G = \kappa^2$ has been added to the energies of the levels for convenience. Type-I levels (full curves) are labelled by their principal quantum number j and their total angular momentum J. Type-II levels (broken curves) are independent of ε_G.

(*a*) Type *A* energy levels exhibit a parabolic tendency to descend for increasing values of the coupling constant. These states have been the subject of the discussion above and are given for stronger coupling by (11).

(*b*) Type *B* energy levels show only slight dependence upon the coupling strength. For sufficiently large principle quantum numbers *B*, these levels are independent of ε_G and in good approximation given by

$$\varepsilon_\delta(I, BJ) = J + 2B + \tfrac{1}{2} - \delta \tag{12}$$

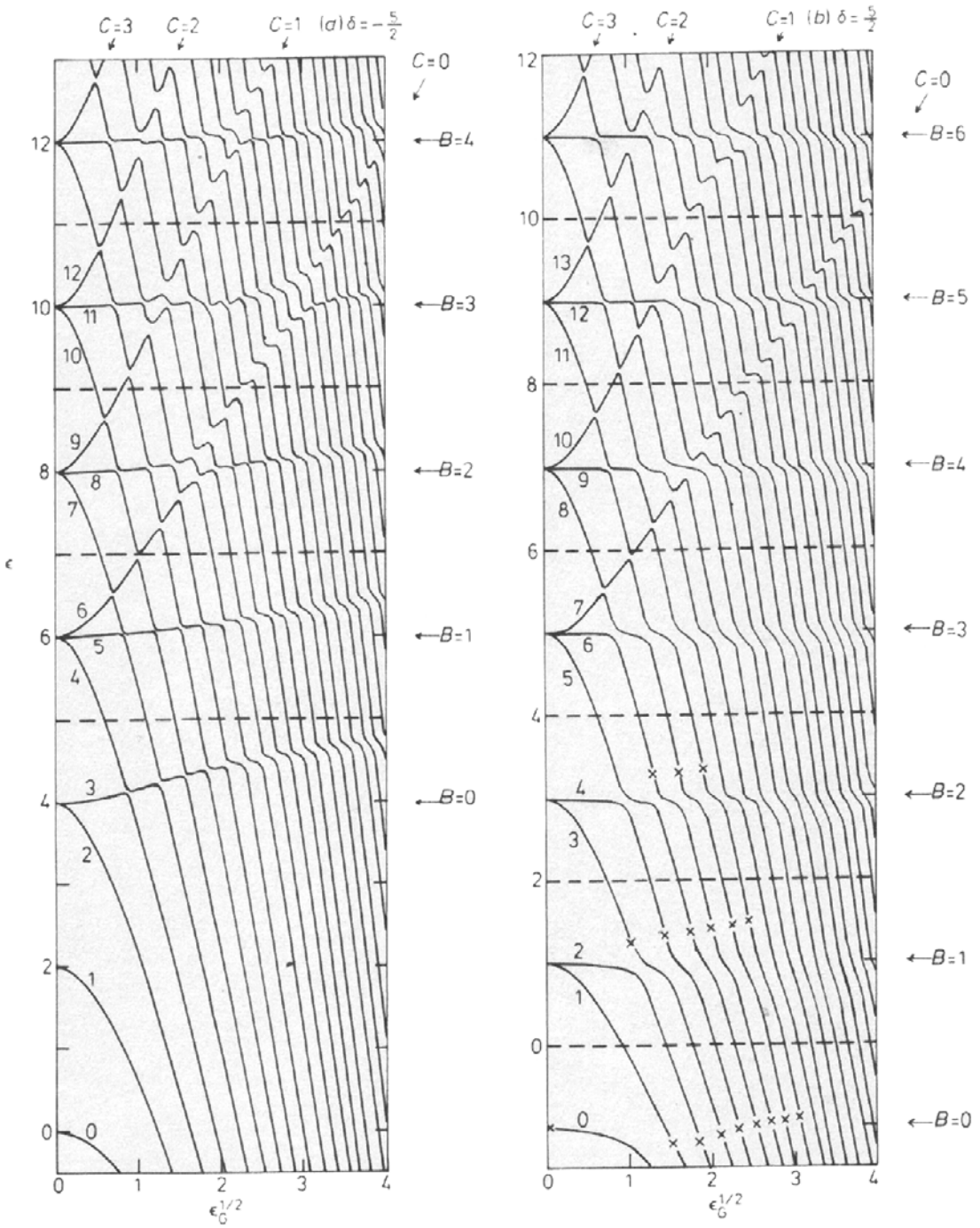

Figure 3. Vibronic energy levels with $J = 1$ versus coupling strength $\varepsilon_G^{1/2}$ for $\delta = -\frac{5}{2}$ (*a*), $\delta = \frac{5}{2}$ (*b*). Full curves represent type-I, broken ones type-II levels. The numbers on the diagrams refer to the *j*-values of the levels. Type *B* and *C* levels are indicated by arrows and denoted with their appropriate quantum numbers. The crosses on some of the levels in (*b*) refer to maxima of the type *B* absorption lines in §4.

where $B = 0, 1, 2, \ldots$, $J = 1, 2, 3, \ldots$. As this expression is identical to the eigenvalues of the p–$(J - 1)$ states of (7), the existence of the type B levels is thought to be mainly due to the influence of these states.

(*c*) Type C energy levels exhibit an ascending tendency for increasing coupling strength. For the range $\frac{1}{2} < |\delta| < 5$ they are well approximated by the upper branch of the hyperbola

$$\varepsilon_\delta(I, CJ) = [1 + (J + 2C - \tfrac{3}{5}|\delta| + 3 + \gamma_1)\varepsilon_G]^{1/2} + J + 2C + |\delta| + \tfrac{1}{2} + \gamma_2 \tag{13}$$

where

$$\gamma_1 = \begin{cases} 0 \\ \frac{1}{2} \end{cases} \quad \text{and} \quad \gamma_2 = \begin{cases} 0 \\ 1 \end{cases} \qquad \text{for} \quad \begin{matrix} \delta > 0.5 \\ \delta < -0.5 \end{matrix}$$

and $C, J, = 0, 1, 2, \ldots$.

3.2.2. The type A, B and C vibronic states can be associated with the lowest, middle and highest adiabatic energy surface of the static problem (§2.2), respectively. In figure 1(*e*) some of the energy levels belonging to these states are indicated. There are of course two degenerate middle surfaces, one of which belongs to the type-II energy levels.

As the coupling strength increases, and $2\varepsilon_G > |\delta|$, the well of the lower energy surface (3) becomes deeper and contains more type A levels. Simultaneously, the highest-energy surface becomes increasingly steeper with the effect that the type C levels are shifted towards higher energies and that the spacing between the levels increases. The middle surface (4) is of course not affected by ε_G but depends on δ. Consequently, type B levels are not expected to depend significantly upon ε_G.

The strong and weak tendencies to form type A, B and C energy levels can be regarded as an intrinsic feature of this pJT system. Whenever the lowest-energy surface lies close to the middle one, as for $\delta > 0$, or close to the middle and upper surfaces, as for $|\delta| \lesssim 0{\cdot}5$, the tendency to form type B, or B and C levels appears to be weak. It is impossible to identify the type A, B and C levels purely by inspecting the behaviour of the energy levels as a function of coupling strength (see §4.1).

4. Optical absorption at zero temperature

We assume that the vibronic states $\Psi_{N'J'M'}(1s)$ associated with the non-degenerate electronic 1s ground state $|1s\rangle \equiv |100\rangle$ have the simple product form

$$\Psi_{N'J'M'}(1s) = |(2N' + J')J'M'\rangle\,|100\rangle \tag{14}$$

with the energies $\varepsilon(N'J', 1s) = -\varepsilon_0 + 2N' + J' + \frac{3}{2}$ where $N', J' = 0, 1, 2, \ldots$. Note that the electronic 1s state lies lower than the zero point of energy (see §2.1) by the energy ε_0, which is assumed to be very much larger than $|\delta|$ and ε_G. As in §2.3 the vibrational states are again eigenvectors of the 3D isotropic oscillator.

The electric dipole moment operator $\boldsymbol{D}$ is for linearly polarised light given by $D_\eta = e\eta$ and its matrix elements between the electronic $|1s\rangle$ and $|2p\rangle$ states are denoted by

$$D = \langle 1s|D_\eta|\eta\rangle \tag{15}$$

where $\eta = x$, y, or z. As the components of the electric dipole moment operator have T_{1u} symmetry and transform in the combined space of electronic and vibrational

coordinates as a set of functions belonging to $J = 1$ with parity $\Lambda' = -1$, non-zero matrix elements occur only between vibronic states of opposite parity for which the difference in J is 0 or ± 1.

For very low temperatures absorption occurs only from the lowest vibronic ground state (14) with $N' = J' = M' = 0$. Electric dipole transitions can then take place only to vibronic type-I states with $J = 1, j = 0, 1, 2, \ldots$, but not to type-II states (see §2.3).

The matrix elements of the electric dipole moment operator between the states (14) and the vibronic type-I states (8) have in the case of $\eta = z$ the general form

$$\langle \Psi^{JM}_{\mathrm{I},j} | D_z | \Psi_{N'J'M'}(1\mathrm{s}) \rangle = D \sum_{N=0}^{\infty} \left[c(J, j, J + 2N - 1) \left(\frac{(J + M)(J - M)}{J(2J - 1)} \right)^{1/2} \delta_{N',N} \delta_{J',J-1} \delta_{M',M} - b(J, j, J + 2N + 1) \left(\frac{(J + M + 1)(J - M + 1)}{(J + 1)(2J + 3)} \right)^{1/2} \delta_{N',N} \delta_{J',J+1} \delta_{M',M} \right] \tag{16}$$

where $c \equiv 0$ for $J = 0$.

For zero temperature the absorption cross section can be written in the form (Dexter 1958, Lax 1952)

$$\sigma(00, \varepsilon) = C \sum_{j=0}^{\infty} | \langle \Psi^{10}_{\mathrm{I},j} | D_z | \Psi_{000}(1\mathrm{s}) \rangle |^2 \delta(\varepsilon(\mathrm{I}, j1) - \varepsilon(00, 1\mathrm{s}) - \varepsilon)$$

where C in the case of a crystalline defect essentially describes the macroscopic effect of the dielectric medium on the absorption centre and is proportional to the energy absorbed in a transition.

The normalised absorption spectrum can now be defined as $I^a_\delta(00, \varepsilon) = \sigma(00, \varepsilon)/CD^2$. With equation (16) we find

$$I^a_\delta(00, \varepsilon) = \sum_{j=0}^{\infty} M^a_\delta(j) \delta(\varepsilon(\mathrm{I}, j1) - \varepsilon(00, 1\mathrm{s}) - \varepsilon) \tag{17}$$

where the strength of the j absorption line is by definition given by

$$M^a_\delta(j) = |c(1, j, 0)|^2 \tag{18}$$

with $j = 0, 1, 2, \ldots$.

4.1. Absorption lines

In figures 4 the strengths of the absorption lines which are associated with the low-energy type-I states with $J = 1$ and main quantum number j are plotted against coupling strength for $\delta = \pm\frac{5}{2}$. There are several groups of absorption peaks which may be associated with the type A, B and C states of §3.

Two situations arise. When the type-I energy levels show a strong tendency to cross, a group of absorption peaks can in good approximation be replaced by an envelope line which is a smooth and continuous function and consists mainly of one or two intensity contributions. In particular, this can be done for the type B and C absorption lines for $\delta \ll -\frac{1}{2}$ (figure 4*a*†) and for the type C lines for $\delta \gg \frac{1}{2}$ (figure 4*b*). Points on an absorption line then correspond to points on the associated type B or C energy level.

† The introduction of the type ($B = 0$) line makes compensational corrections of the type A lines necessary.

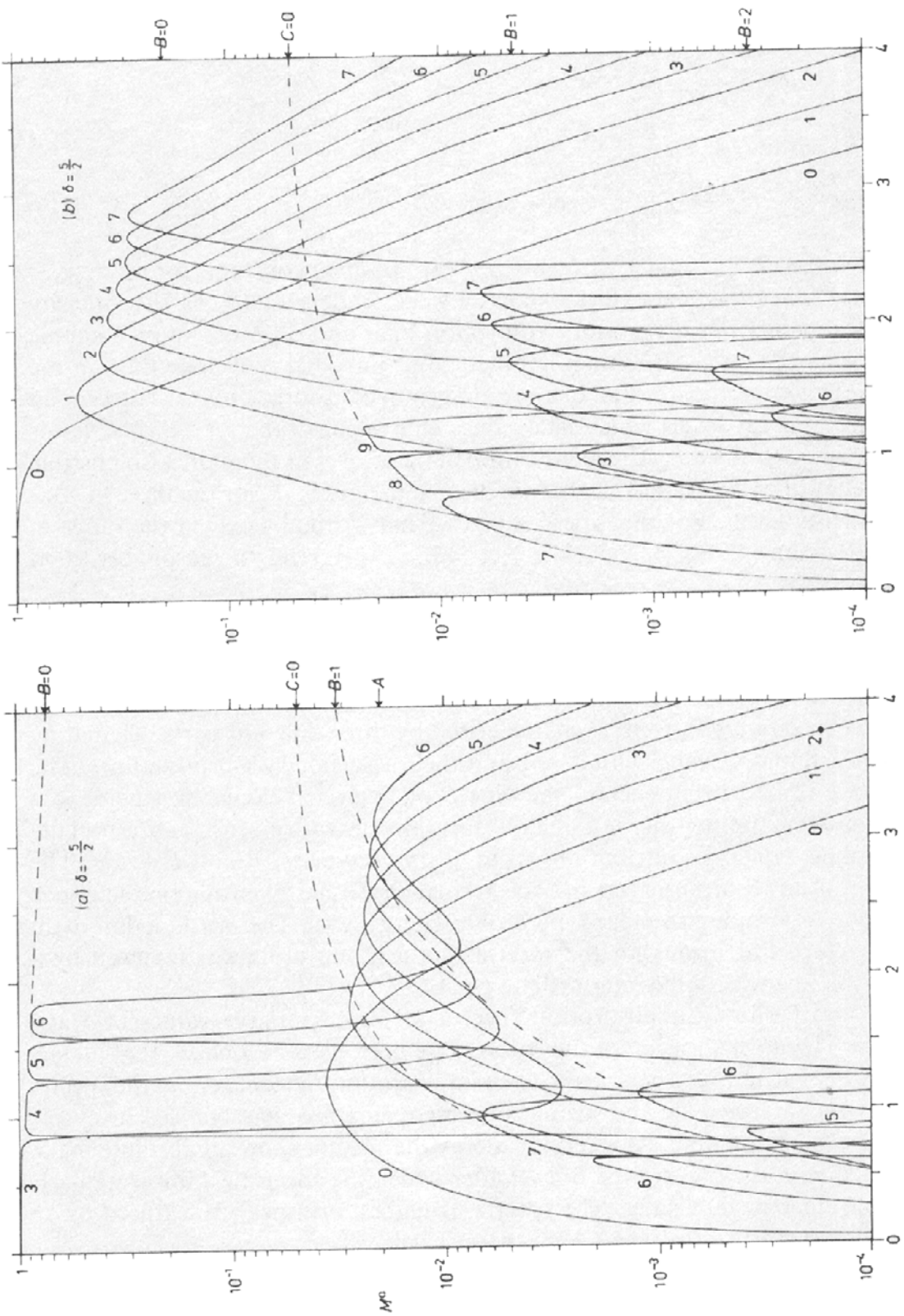

Figure 4. Strengths of absorption lines versus $\epsilon_G^{1/2}$ for $\delta = -\frac{5}{2}$ (*a*) and $\delta = \frac{5}{2}$ (*b*). The lines are labelled by the principal quantum number j of the corresponding type-I states with $J = 1$. The arrows on the right-hand side indicate type *A*, *B* and *C* absorption lines. The type *B* and *C* lines with given quantum numbers each refer to a group of absorption maxima; for strong tendency of energy levels crossing the associated envelope absorption lines are drawn (broken lines).

The case $\delta = -\frac{1}{2}$ (not shown) can at least for weak coupling be regarded as a reference point of the spectra as in this case the lowest ($J = 1$) states at $\varepsilon_G = 0$ are the degenerate s–J and p–($J - 1$) states of (7) with $N = 0$.

The intensities of the type A, B and C absorption lines follow approximately the expressions

$$P_A(\varepsilon_G) = \alpha_1 \varepsilon_G^{A+1} \exp(-\beta_1 \varepsilon_G)$$

$$P_{B=0}(\varepsilon_G) = (1 - \alpha_2) \exp(-\beta_2 \varepsilon_G) + \alpha_2$$

$$P_{C \text{ or } B \geqslant 1}(\varepsilon_G) = \alpha_3 [1 - \exp(-\beta_3 \varepsilon_G)] \tag{19}$$

where $A, B, C = 0, 1, 2, \ldots$, and α_i, β_i ($i = 1, 2, 3$) are positive constants for given δ.

Alternatively, when the energy levels shows a weak tendency to cross, the intensity overlap consists mainly of two or more absorption lines and does not show a simple functional dependence on ε_G. It is then impractical to introduce envelope lines in the above manner. However, the maxima of a certain group of absorption lines correspond to points on the j-energy levels which lie on lines equivalent to the type B or C levels and with similar ε_G dependence. An identification of these levels is therefore also possible for weak tendency of crossing, and has been indicated in figure 3(*b*) for the three lowest-lying type B energy levels. For the type C levels we may formally extend the range of validity of expression (13) to $|\delta| < \frac{1}{2}$, where $\gamma_1 = 0$, $\gamma_2 = 1$ yields a reasonably good approximation.

4.2. Absorption spectra

The absorption spectra are in general characterised by three different parts originating from the type A, B and C states with $J = 1$ and their associated absorption lines. The discussion above revealed that each of the type B or C levels belongs in general to a group of lines and that the intensity of a single absorption line with given ε_G can, especially for weak coupling, contain contributions from all three type A, B and C levels. The spread in energy of an absorption peak in a spectrum may thus be taken as a characteristic for the tendency to form a particular type B or C energy level. The introduction of an absorption envelope line means for the spectra that a group of lines is replaced by a single absorption line with some intermediate position.

Figures 5 and 6 show the absorption spectra for representative values of δ and $\varepsilon_G = 1$ and 16. The normalisation of the spectra has been used as a check that all significant intensity contributions have been taken into account. At low energies the spectra of particularly the intermediate and strong coupling region are characterised by evenly spaced type A absorption lines. At a certain energy the spectra show an absolute maximum associated with the lowest type B level after which the spectra exhibit irregularly spaced lines of different intensities. The spectra at highest energies are featured by an intensity peak belonging to the type $C = 0$ energy level.

Whenever the lowest adiabatic energy surface is far away from the two upper ones, type A absorption lines appear at the low-energy end of the spectra. In particular, this is the case for $\delta \ll -\frac{1}{2}$ at all coupling strengths. The type A lines exhibit a distribution, the maximum of which is shifted towards lower energies and larger values of quantum number A as ε_G becomes larger and the adiabatic well deeper (fixed δ). The width of this distribution increases for increasing coupling strength. In the strong-coupling region

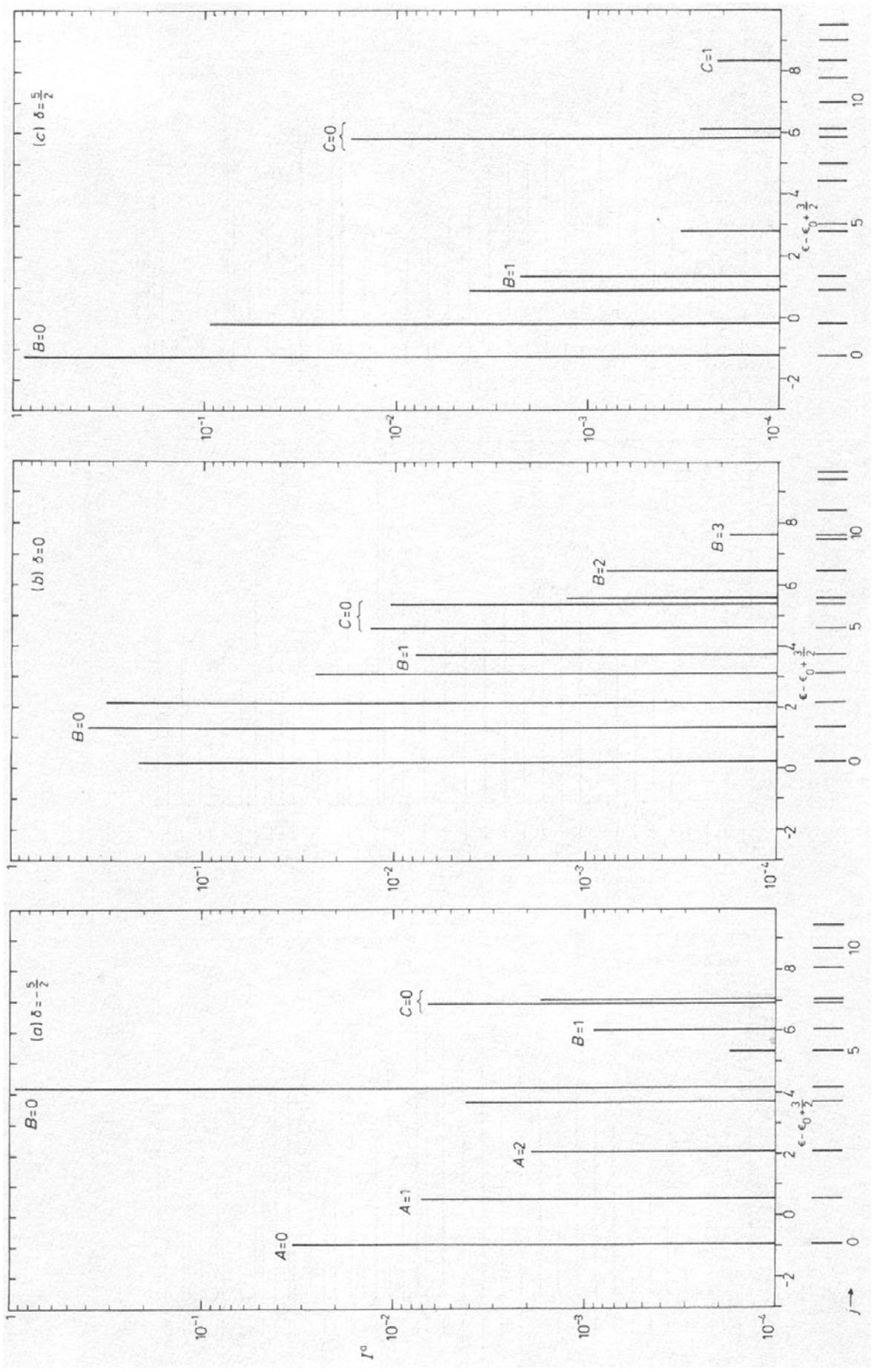

Figure 5. Normalised absorption spectra at $T = 0$ K for $\varepsilon_G = 1$ and $\delta = -\frac{5}{2}$ (*a*), $\delta = 0$ (*b*), and $\delta = \frac{5}{2}$ (*c*). $I^{\alpha}_{\beta}(00, \varepsilon)$ of (17) has been plotted against $\varepsilon - \varepsilon_0 + \frac{3}{2}$ and each absorption line is labelled by its j-value. Whenever possible, absorption peaks with $B = 0, 1, 2, 3$ and $C = 0, 1$ have been indicated. Similarly, type A lines have been denoted whenever identified.

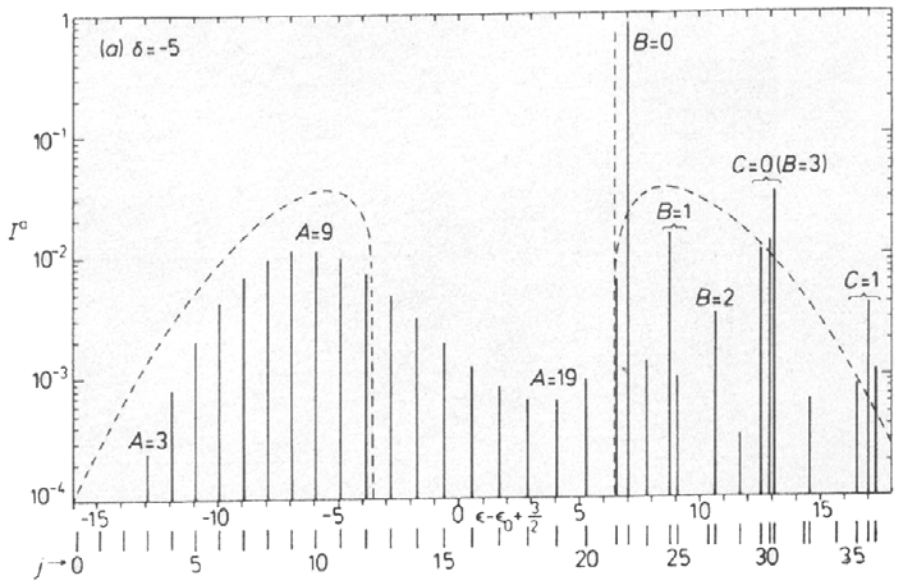
(a) δ=-5
B=0
C=0(B=3)
B=1
B=2
C=1
A=9
A=19
A=3
I^a
$\epsilon-\epsilon_0+\frac{3}{2}$
j→

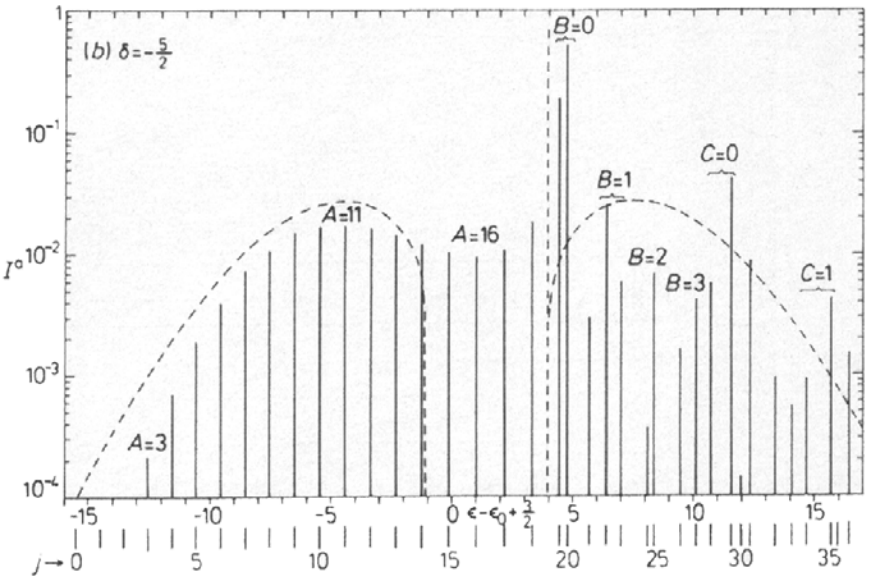
(b) δ=-5/2
B=0
C=0
B=1
A=11
A=16
B=2
B=3
C=1
A=3
I^a
$\epsilon-\epsilon_0+\frac{3}{2}$
j→

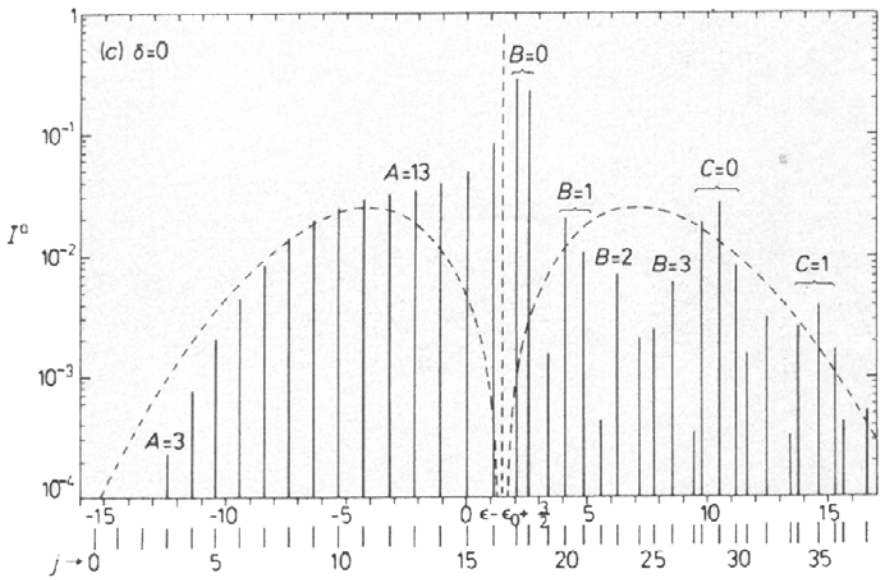
(c) δ=0
B=0
A=13
C=0
B=1
B=2
B=3
C=1
A=3
I^a
$\epsilon-\epsilon_0+\frac{3}{2}$
j→

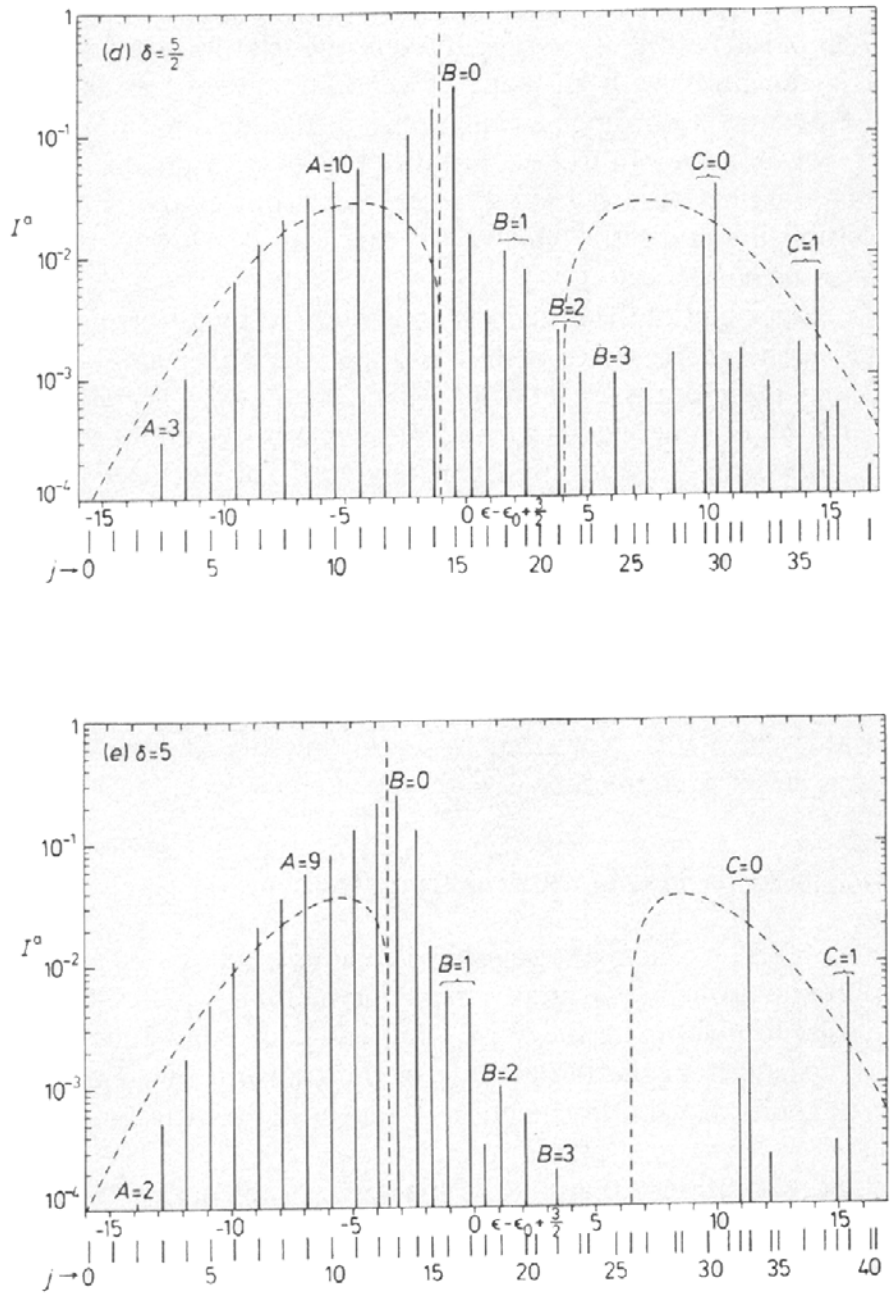

Figure 6. Normalised absorption spectra at $T = 0$ K for $\varepsilon_G = 16$ and $\delta = -5$ (*a*), $\delta = -\frac{5}{2}$ (*b*), $\delta = 0$ (*c*), $\delta = \frac{5}{2}$ (*d*), and $\delta = 5$ (*e*). $I^a_\delta(00, \varepsilon)$ of (17) has been plotted against $\varepsilon - \varepsilon_0 + \frac{3}{2}$ and each absorption line is labelled by its j-value. Whenever possible, absorption peaks with $B = 0, 1, 2, 3$ and $C = 0, 1$ have been indicated. Similarly, type A lines have been denoted whenever identified. The notation in (*a*), for instance, means that all lines at the low-energy end of the spectrum up to and including $j = A = 19$ have predominantly type A character. The broken lines represent the semiclassical absorption lineshape function.

the distribution resembles a Poisson distribution with approximately equidistant lines of energy separation 1 (see also figure 1*e*).

The type *B* states with $J = 1$, and the middle energy surface, can be associated with a series of absorption peaks, the positions of which are given by the energies of these states. Because of the nature of the type *B* levels, the relative positions of these peaks do not change significantly with ε_G, and the separation of the peaks is approximately equal to 2. However, according to equation (12) the absolute positions of the peaks depend on $(-\delta)$. Because of this circumstance the lowest type *B* absorption peaks can overlap the type *A* lines in such a way that, even in strong coupling, a type *A* absorption peak is not visible in the spectra, which is the case when the lowest and middle adiabatic energy surfaces lie close.

The high-energy end of the spectra is characterised by absorption peaks which can be associated with type *C* states with $J = 1$ and the upper adiabatic energy surface. The positions of these peaks are of course given by the type *C* energy levels which are shifted towards higher energies as ε_G and $|\delta|$ increases (see equation (13)). The separations of the peaks are $\gtrsim 2$ and approximately constant for given ε_G but increase for increasing values of ε_G. Note that at $\delta \gg \frac{1}{2}$ and strong coupling, i.e. when the lowest and middle energy surfaces are far away from the highest one, the spectra are characterised by an 'energy gap' of extremely low intensity (figure 6*e*).

From figures 5 and 6 it can be seen that the type $(B = 0)$ absorption peak carries about 99 to 70 % of the total intensity and the type *A* peak up to 10 or 20 %. The intensities of all other peaks are less and increase for increasing coupling strength but decrease for increasing values of $\delta > 0$. Note that in weak coupling and for $\delta \ll -\frac{1}{2}$ the type *A* contribution is larger than the type $C = 0$ one, but vice versa for $\delta \gg \frac{1}{2}$.

5. Absorption lineshape in semi-classical approximation

For the $(s + p) \otimes T_{1u}$ system the lineshape function may be calculated in the semi-classical approximation by essentially the same method which Toyozawa and Inoue (1966) have used to investigate the absorption bands of Jahn–Teller systems. However for the heavy particles in the initial state of the transition we employ the quantum-statistical probability distribution function P_g instead of the high-temperature Boltzmann distribution.

As the energy solutions (3) and (4) of the static problem depend only on the radial coordinate q, it is of advantage to introduce the polar coordinates (q, θ, φ) also for P_g. The vibronic states associated with the electronic ground state have the product form (14). P_g is therefore the probability distribution for the 3D isotropic oscillator, which can be derived from the formulae given by Landau and Lifschitz (1967, §§ 28, 30) for the 1D harmonic oscillator. The quantum mechanical probability that when the system is in the initial electronic ground state it will be found in the volume element $d\Omega = d\varphi d\theta \sin\theta \, dq \, q^2$ of phase space is represented by $dW_\Omega = P_g d\Omega$ where $P_g = (b/\pi)^{3/2} \times \exp(-bq^2)$ and $b = \tanh(1/2\beta)$, $\beta = kT/\hbar\omega$. At high temperatures ($b \approx 1/2\beta$), P_g is the classical Boltzmann distribution within the energy continuum of the initial electronic state. At low temperatures ($b \approx 1$) P_g takes the form of the quantum probability distribution for the coordinate in the ground state of the oscillator.

The normalised absorption lineshape function is found to be

$$I^a(\varepsilon) = \tfrac{1}{3} \sum_i \int_0^{2\pi} d\varphi \int_0^{\pi} d\theta \sin\theta \int_0^{\infty} dq q^2 \, P_g \delta(\varepsilon_i(q) - \varepsilon_g(q) - \varepsilon)$$

where the adiabatic energy surfaces ε_i are given by (3) and (4) and $\varepsilon_g = -\varepsilon_0 + q^2/2$. Integration and summation can then be carried out by making use of the properties of the delta-function:

$$I^a(\varepsilon) = I_1^a(\varepsilon) + I_2^a(\varepsilon) \tag{20}$$

where

$$I_1^a(\varepsilon) = \tfrac{1}{3}(2\pi)^{-1/2}(b/\varepsilon_G)^{3/2}\left[(\varepsilon - \varepsilon_0)^2 - \delta^2\right]^{1/2}|\varepsilon - \varepsilon_0| \exp\{-[(\varepsilon - \varepsilon_0)^2 - \delta^2]b/2\varepsilon_G\}$$

$$\text{for } |\varepsilon - \varepsilon_0| \geqslant |\delta| \ .$$

and

$$I_2^a(\varepsilon) = \tfrac{2}{3}\delta(\varepsilon - \varepsilon_0 + \delta) \qquad \text{for } -\infty < \varepsilon < +\infty.$$

The spectrum consists of three parts in accordance with the three different adiabatic energy surfaces: a delta function of constant strength and two wings which show reflection symmetry to each other and have a gap of $2|\delta|$ between them where the absorption intensity is zero. Each wing carries $\frac{1}{6}$ of the total intensity.

For strong coupling and/or high temperatures, i.e. for $x/2 \ll 1$ where $x = b\delta^2/2\varepsilon_G$, the positions, magnitude of the maxima of the wings, and width at half maximum are given by

$$\begin{aligned}
\varepsilon_{\max 1,2} &= \varepsilon_0 \pm [(1 + x/2)2\varepsilon_G/b]^{1/2} \\
I^a_{\max} &= (1/3e)(2b/\pi\varepsilon_G)^{1/2}(1 + x/2) \\
\Delta &= \tfrac{7}{6}(2\varepsilon_G/b)^{1/2}(1 - x/3).
\end{aligned} \tag{21}$$

For $\delta = 0$ the expressions for $\varepsilon_{\max}$ and $I^a_{\max}$ are exact for all ε_G and T.

The lineshape function (20) has been drawn in figures 6 for $\varepsilon_G = 16$ and various values of δ (broken lines). In the same way as the lowest, middle and upper adiabatic energy surfaces can be associated with the type A, B and C absorption peaks, respectively, the three semclassical contributions correspond to these peaks and can be denoted accordingly.

Turning first to the low-energy type A wing, we find good agreement with the computed spectra as regards the position of the maximum, where the accuracy improves as $|\delta|$ becomes smaller. However, the magnitude of the maximum, the width and the area of the wing are given in good approximation only for $\delta > 0$. The delta function of (20), which corresponds to all of the type B absorption peaks, is placed close to the centre of gravity of the type ($B = 0$) peak, particularly in the case of $\delta \gtrsim -\frac{1}{2}$. Note that the delta function takes into account only some fixed part of the total type B intensity with best agreement reached for $\delta \gtrsim 0$. Finally we find that the high-energy type C wing is only roughly related to the type C peaks. However, the gap between the type A and C wings (for $\delta \neq 0$) exhibits itself in the spectra as a drop in intensity, especially for large δ.

6. Discussion and conclusions

Our computational results suggest that a factorisation of the type-I vibronic states does not only occur for the low-energy states in the strong-coupling region (Ham 1973, Grevsmühl 1981, §4.1), but also in good approximation for the high-energy states at all coupling strengths whenever the energy levels with the same J show strong tendencies

to cross. It is then useful to classify the type-I states into three further types with quantum numbers A, B and C which can be associated with the lowest, middle and upper energy surface of §2.2, respectively.

Moreover, the analysis of the individual absorption lines versus coupling strength reveals that, in general, a group of absorption peaks can be associated with either one of the type B or C energy levels, or with all the type A levels, with $J = 1$. This circumstance makes the introduction of type A, B and C levels also useful for weak tendency of levels crossing, enabling a unified description of the absorption spectra for all values of δ and ε_G.

O'Brien (1976) developed a method based on the WKB approximation and calculated the higher energy levels as

$$\begin{aligned} \varepsilon(\mathrm{I}, A) &= A + \tfrac{1}{2} - \varepsilon_G \\ \varepsilon(\mathrm{I}, BJ) &= J + 2B + \tfrac{1}{2} - \delta \end{aligned} \tag{22}$$

where $A, B = 0, 1, 2, \ldots$, and $J = 1, 2, 3, \ldots$. The first expression which is valid only under the condition $\varepsilon \gg 2\delta$, describes the type A energy levels of §3.2 and corresponds to equation (11). Best agreement with the computed levels is found for $|\delta| \lesssim \frac{1}{2}$, $\varepsilon_G > 1$, and energies $\varepsilon > 6$, as expected. The second expression is identical to the energies (12) of the type B states. It has been obtained under the condition $(\varepsilon + \delta) \gg 1$, which is clearly demonstrated in figures 2. No type C states appear in O'Brien's calculation. This has to be expected as her calculation incorporates the conditions of the strong-coupling limit ($2\varepsilon_G \gg |\delta|$, $\varepsilon_G \gg 1$), and the solutions apply only to small $|\delta|$, which is in agreement with our computational results. Even when extending this method to larger values of $|\delta|$, we expect better results for $\delta < 0$ than for $\delta > 0$, as the WKB approximation does not give good results when the energy surfaces lie close, which also agrees with our comments on the strong/weak tendencies of the vibronic energy levels to cross (see §3.2).

The absorption lines (figure 4) show a pronounced resonance structure as the coupling strength is varied. In general, resonance points of zero intensity occur between type B absorption lines at the energies $\varepsilon^B_{\mathrm{res}} = \frac{7}{2} + 2B - \delta$, where $B = 0, 1, 2, \ldots$. However, whenever type C and B levels lie very close, we expect some interference between their associated absorption lines, and the minimal points may only be relative. Similarly, for $\delta \ll -\frac{1}{2}$, the absorption lines exhibit pronounced relative minima when changing from a type ($B = 0$) state to a type A state behaviour (figure 4*a*). The associated resonance energies are then approximately given by $\varepsilon^A_{\mathrm{res}} = 2 - \delta - \varepsilon_G^{1/2}$.

From the investigations of an ideal Jahn–Teller system (Grevsmühl and Wagner 1973) we conclude that the optical resonance effect is a direct consequence of the dynamic pJT effect, reflecting the fact that the effective splitting of the purely electronic levels can be of the same order of magnitude as the elementary phonon excitations. In particular, at the resonance points energy may be exchanged between the electronic and nuclear system which will affect the transition probabilities. When both systems are completely in resonance, we expect the absorption intensity to drop to zero at the frequency which corresponds to the exchange (resonance) energy. Note that for strong tendency of energy levels crossing, i.e. when the energy surfaces are far apart, the absorption lines may be replaced by envelope lines, and the resonance effect may then be neglected (figure 4).

Recently, Kayanuma and Kojima (1980) have used the method of numerical diagonalisation of the vibronic Hamiltonian to calculate the absorption spectra for

$\delta = 0$ and $+5$ and various values of the coupling constant. Whenever comparable, our results are found to be in complete agreement with theirs.

The method of numerical diagonalisation has also been applied to the non-degenerate and doubly denenerate pJT systems (Natsume 1976). The absorption spectra of these systems show a remarkable resemblance to the spectra above. For the same parameters, best agreement is found for the low-energy lines, particularly for large $|\delta|$ and/or strong coupling, which agrees with the fact that the adiabatic energy surfaces of all three cases show a qualitatively similar behaviour but differ, of course, in regard to their number and dimensionality.

Acknowledgments

The author wishes to express his sincere thanks to Dr M C M O'Brien for many helpful discussions and her continuous encouragement throughout this work. This research was partially supported by the Foundation of the Florey European Studentships, Queen's College, Oxford.

References

Dexter D L 1958 *Solid St. Phys.* **6** 352 (New York: Academic Press)
Grevsmühl U 1976 *DPhil thesis* University of Oxford
—— 1981 *J. Phys. C: Solid State Phys.* **14** 685–96
Grevsmühl U and Wagner M 1973 *Phys. Stat. Solidi* (b) **58** 139
Ham F S 1973 *Phys. Rev.* B **8** 2926
Ham F S and Grevsmühl U 1973 *Phys. Rev.* B **8** 2945
Heine V 1964 *Group Theory in Quantum Mechanics* (Oxford: Pergamon)
Kayanuma Y 1976 *J. Phys. Soc. Japan* **40** 363
Kayanuma Y and Kojima T 1980 *J. Phys. Soc. Japan* **48** 1990
Kayanuma Y and Toyozawa Y 1976 *J. Phys. Soc. Japan* **40** 355
Landau L D and Lifshitz E M 1967 *Statistical Physics* (Oxford: Pergamon)
Lax M 1952 *J. Chem. Phys.* **20** 1752
Messiah A 1969 *Quantum Mechanics* vol I and II (Amsterdam: North-Holland)
Natsume Y 1976 *J. Phys. Soc. Japan* **41** 607, 615
O'Brien M C M 1976 *J. Phys. C: Solid State Phys.* **9** 2375
Pooler D R 1980 *Phys. Rev.* B **21** 4804
Toyozawa Y and Inoue M 1966 *J. Phys. Soc. Japan* **21** 1663
Wybourne B G 1974 *Classical Groups for Physicists* (New York: Wiley)